Aptamer-conjugated liposome system for targeting MUC1-positive cancer: an in silico screening approach

Md Shakil Ahmed Khan[1†], Jiwoo Park[1†], Somin Lee[1†], Jee-Eun Hwang[1], Chiwoo Oh[2], MinKyu Kim[2], Jeong-Seob Lee[2], Jongyeong Jeon[1], Beomjin Park[1], Shengjun Li[1], Han Na Jung[2] and Hyung-Jun Im[1,2,3,4*]

Abstract

This study aims to overcome the adverse effects of conventional cytotoxic chemotherapy on healthy organs by developing a target-specific approach utilizing Doxorubicin (DOX)-encapsulated liposome conjugated with aptamer which has high binding affinity to the overexpressed Mucin-1 (MUC1) protein in various cancer types. To ensure optimal aptamer selection, we conducted a comprehensive in silico comparison of several MUC1-targeting aptamers, including 5TR1, MA3, S1.6, S2.2, and STRG2. As a results, the S1.6 aptamer was selected as a targeting ligand by comparing the thermodynamic stability, docking score, confidence score, and binding affinity. Also, spectrophotometer, gel electrophoresis, and Dynamic light scattering (DLS) confirm the size, zeta potential, DOX encapsulation rate, stability, and aptamer conjugation of liposomes. In addition, flow cytometry results validate MUC1 expression in MCF7 cells while not in MDA-MB-231 cells, while confocal microscopy confirmed the specific cellular uptake of the lipo-aptamer complex. Consequently, this aptamer-mediated liposomal drug delivery approach shows potential for enhancing the specificity and reducing the side effects of conventional chemotherapy, while the use of in silico methods provides an efficient and cost-effective strategy for screening and optimizing aptamer candidates, simplifying the overall development process. Further in vivo evaluation for therapeutic efficacy and clinical applications is warranted.

Keywords Chemotherapy, Liposome, Doxorubicin, Aptamer, MUC1 protein, Cancer cells

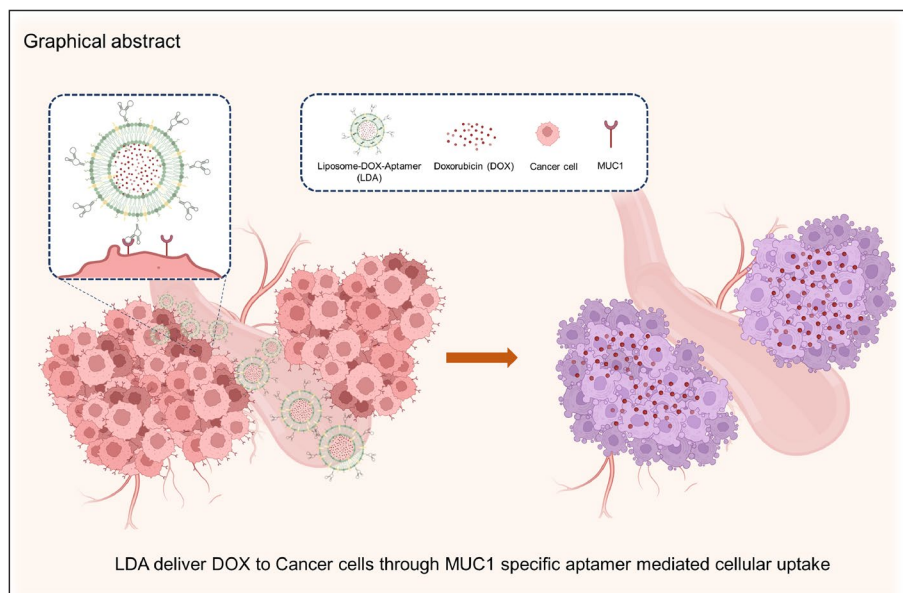†Md Shakil Ahmed Khan, Jiwoo Park and Somin Lee contributed equally to this work.

*Correspondence:
Hyung-Jun Im
iiihjjj@snu.ac.kr
Full list of author information is available at the end of the article

Graphical Abstract

Graphical abstract

Liposome-DOX-Aptamer (LDA)   Doxorubicin (DOX)   Cancer cell   MUC1

LDA deliver DOX to Cancer cells through MUC1 specific aptamer mediated cellular uptake

Introduction

Nano-particle-based drug delivery systems have garnered significant attention in cancer research as a promising approach to enhance the effectiveness of cancer treatment [1]. These systems minimize the adverse effects of traditional non-target-specific cytotoxic chemotherapeutic agents on normal organs. Among the available nanocarrier systems, liposomes have emerged as highly promising platforms for controlled and targeted drug delivery to cancer cells due to their customizable characteristics, such as size, surface charge, and lipid composition, allowing for tailoring and optimization to meet specific treatment requirements [2–5].

Liposomes are vesicles composed of phospholipids, featuring a bilayer membrane structure similar to biological membranes as well as it is easy to synthesize, time efficient, and cost-effective [2, 4]. They hold significant potential for improving the therapeutic effectiveness of anticancer agents by increasing drug concentrations within tumor cells while minimizing exposure to normal tissues [2, 6–8]. Liposomes are enabled with desired attributes for improved drug encapsulation, stability, and release kinetics. Additionally, liposomes exhibit biocompatibility and provide an ideal surface for attaching targeting ligands like antibodies, peptides, and aptamers [9]. Notably, liposomal formulations have already received clinical approval for various anticancer drugs [10].

However, in 2016, Petersen et al. provided evidence that conventional PEG(Poly ethylene glycol)ylated liposomes carrying chemotherapeutic agents showed only limited improvement in clinical effectiveness compared to chemotherapeutics administered without a delivery vehicle [11]. Furthermore, the potential benefits of carrier-mediated chemotherapy, such as the Enhanced permeability and retention (EPR) effect and the tumor microenvironment, have not translated into enhanced clinical efficacy. Challenges such as determining the optimal specificity for carrier-mediated agents and the lack of standardization in their implementation have hindered their success in clinical studies [11]. To address this limitation, researchers have developed a technique that involves attaching targeting ligands to the surface of liposomal vehicles. This approach, named targeted drug delivery system, aims to improve the specificity of drug delivery to cancer cells.

In addition, among all those targeting ligands, aptamers have recently emerged as a novel and promising tool for targeted drug delivery applications because of their desirable characteristics such as high target specificity, ease of synthesis, thermodynamic stability, and non-immunogenicity [12, 13]. The production process of aptamers occurs outside of biological systems, minimizing the risk of viral or bacterial contamination [14, 15]. Unlike antibodies, aptamers lack the Fc region, eliminating the potential for immune system stimulation upon systemic

Khan *et al. Health Nanotechnology*   (2025) 1:2

Page 3 of 14

administration. Moreover, aptamers demonstrate superior tumor penetration, retention, and homogeneous distribution compared to antibodies and peptides [15, 16]. Their smaller size facilitates enhanced tumor penetration, overcoming a challenge faced by antibodies and peptides that often require size optimization [17]. Furthermore, attaching aptamers to nanoparticle surfaces is more amenable and reproducible compared to antibody attachment [7, 18]. Consequently, in the field of oncology, aptamers offer distinct advantages over antibodies and peptides.

As a targeting receptor, MUC1, a transmembrane glycoprotein, is frequently overexpressed in several epithelial adenocarcinomas, making it a prominent biomarker in cancer research [19–23]. The prevalence of overexpression is particularly noteworthy, with approximately 65% of newly diagnosed tumors in the United States displaying elevated levels of MUC1 [24]. It is highly expressed in lung, liver, colon, breast, pancreatic, and ovarian cancers [25]. Such a high occurrence makes it an attractive and viable target for tumor antigen-directed approaches in cancer diagnosis, treatment, and management [22]. As an essential oncogene, it plays a significant role in regulating numerous cancer-related processes, including cell growth, proliferation, metastasis, apoptosis, and developmental pathways [22, 23, 25]. The upregulation of MUC1 in cancerous tissues is a remarkable feature, as its expression levels can be 10–40 times higher compared to normal tissues [22]. Furthermore, MUC1 exhibits distinct glycosylation patterns, with neoplastic tissues showing under-glycosylation while healthy cells display high glycosylation [26, 27]. This disparity in glycosylation profiles provides an opportunity to differentiate cancerous cells from normal cells, presenting potential avenues for targeted drug delivery strategies [26, 27].

Numerous cancer-targeting aptamer-conjugated liposomes have already been developed by modifying them with aptamers that exhibit specific interactions with highly expressed MUC1 in cancer cells [28–30]. This "Aptabase: An aptamer database" provided us with a list of five aptamers, namely 5TR1, MA3, S1.6, S2.2, and STRG2, all of which have been previously reported to target the MUC1 protein. Moosavian et al. in 2019 investigated the therapeutic effectiveness of a 5TR1 aptamer-conjugated liposomal DOX delivery system targeted to MUC1, showing enhanced tumor accumulation and improved survival in mice [31]. Furthermore, Kim et al. developed dual-aptamer-conjugated liposomes for targeted delivery of DOX to breast cancer cells and cancer stem cells, resulting in increased cytotoxicity and inhibition of metastasis in 2019 [32]. Similarly, the MA3 aptamer has also been investigated to target MUC1 in previous works. These include the

use of self-assembled DNA–protein hybrid nanospheres as biocompatible Nano-drug carriers [33] and the enhancement of thermal damage by iron nanoparticles [34]. The S2.2 aptamer, on the other hand, has been extensively studied and utilized for targeting MUC1. Mohapatra et al. developed S2.2 aptamer-conjugated liposomes, demonstrating synergistic anticancer effects and inhibition of tumor growth in 2017 [35]. It has been also used in various approaches, such as using silica nanoparticles to overcome Navitoclax resistance [36], targeted SPION siderophore conjugate loaded with DOX [37], and delivery of epirubicin using ferritin nanoparticles [38]. Additionally, in silico studies conducted by Santini et al. and Rhinehardt et al. have shown promising results for the S2.2 aptamer [39, 40]. While previous studies have demonstrated the therapeutic potential of various MUC1-targeting aptamers, they have typically focused on individual aptamers without conducting a comprehensive comparison across multiple candidates. In contrast, our study employed an in silico approach to systematically evaluate and screen MUC1-targeting aptamers. By assessing key parameters such as thermodynamic stability, docking score, confidence score, and binding affinity, we were able to rank the aptamers based on their suitability for targeted drug delivery. This evaluation process enhances the robustness and objectivity of aptamer selection while offering a more efficient and cost-effective strategy for optimizing candidates, addressing a limitation in prior research. After this detailed screening, we developed aptamer-conjugated liposomal systems and evaluated their cellular uptake, allowing us to investigate the feasibility of these systems for targeted drug delivery to MUC1-expressing cells. This approach represents a significant advancement toward improving the specificity and efficacy of cancer treatments.

Results and discussions
Aptamer modeling
To perform the comparative analysis among the MUC1 targeted aptamers, we utilized the "UNAFold" web server to generate the Two-dimensional (2D) of the aptamers which represents the Gibbs free energy change associated with the folding and hybridization of nucleic acid sequences [41]. During the 2D structure prediction, the targeted aptamers, namely S1.6, 5TR1, MA3, S2.2, and STRG2, provided the dG score of -2.27, -2.00, -8.62, -1.57, and -2.67, respectively (Table 1). A lower dG score suggests a more stable structure or stronger hybridization between nucleic acid strands [41]. Figure 1A–E represent the 2D structures of the aptamers. In addition, Fig. 1F–J depict the first predicted Three-dimensional (3D) model

Khan *et al. Health Nanotechnology*   (2025) 1:2

Page 4 of 14

Table 1 Aptamer sequences and scoring metrics

Aptamer Name	Aptamer Sequence 5′ to 3′	Ionic conditions of binding buffer	dG score	Docking Score	Confidence Score	Affinity (nM)
5TR1	GGGAGACAAGAATAAACGCTCAAG AAGTGAAAATGACAGAACACAACAT TCGACAGGAGGCTCACAACAGGC	100 mM Na^+ 5 mM Mg^{2+}	-2.00	-296.36	0.9492	47.3
MA3	AACCGCCCAAATCCCTAAGAGTCG GACTGCAACCTATGCTATCGTTGAT GTCTGTCCAAGCAACACAGACACA CTACACACGCACA	140 mM Na^+ 1 mM Mg^{2+}	-8.62	-279.99	0.9308	38.3
S 1.6	GGGAGACAAGAATAAACGCTCAAG CAACAGGGTATCCAAAGGATCAAAT TCGACAGGAGGCTCACAACAGGC	700 mM Na^+	-2.27	-286.72	0.9390	0.2131
S 2.2	GCAGTTGATCCTTTGGATACCCTGG	140 mM Na^+	-1.57	-251.94	0.8848	0.135
STRG2	GAGACAAGAATAAACGCTCAAGGCT ATAGCACATGGGTAAAACGACTTCG ACAGGAGGCTCACAACAGGC	150 nM Na^+ 5 nM Mg^{2+}	-2.67	-279.06	0.9296	18.6

This table displays the following information: the names of the aptamers, their ionic conditions of binding buffer, dG scores of 2D modeling, as well as the binding affinity, docking score, and confidence score of the lipo-aptamer and MUC1 interaction

for each aptamer obtained from the Xiao Lab web server [42, 43]. These 3D models were minimized and refined by Maestro 12.5 software for molecular docking.

Molecular docking

In the molecular docking process to screen the aptamers against the MUC1 protein, we utilized the HDOCK SERVER, renowned for its proficiency in DNA–protein molecular docking. This approach provided the 3D model data visualized in Fig. 1K–O, illustrating the docking simulations between various aptamers and MUC1. Also, the HDOCK SERVER provided docking scores and confidence scores for the DNA–protein complexes [44]. As the lowest docking score means better interaction, examining Table 1, it is evident that the docking score of S1.6 is better than that of MA3, S2.2, and STRG2 while being slightly lower than 5TR1. These scores provide insight into the binding affinity and strength between the aptamers and the protein.

In addition to docking scores, confidence scores were also obtained to estimate the reliability of the predicted complexes. Higher confidence scores indicate a higher level of confidence in the predicted interactions. The maximum confidence score is 1.00, and in our case, 5TR1 showed the best score which is 0.9492 and the second best is S1.6 exhibited a confidence score of 0.9390.

Aptamer selection

A comprehensive analysis of various parameters was conducted including docking scores, confidence scores, binding affinity, and dG scores, to compare different aptamers and visualized through radar charts (Figure S1, 2). Despite our study showing only a slightly superior outcome of 5TR1 in terms of docking and confidence scores, S1.6 demonstrated significantly better binding affinity and dG score. Notably, while 5TR1 exhibited a binding affinity of 47.3 nM, S1.6 displayed a substantially lower value of 0.2131. This considerable disparity emphasizes the remarkable superiority of S1.6 over 5TR1.

Although MA3 exhibits a better dG score in our study, it falls short in other parameters such as docking score, confidence score, and binding affinity when compared to S1.6. As a result, S1.6 emerged as a more favorable choice over MA3.

During our study, S2.2 exhibited lower scores in all parameters except for binding affinity. Additionally, the difference between S2.2 and S1.6 in terms of binding affinity is only 0.078, which can be considered negligible. Therefore, once again, S1.6 proves to be the superior choice over S2.2.

Both S1.6 and STRG2 lack prior research, making them suitable candidates for further study (Figure S3). Furthermore, considering the binding affinity, docking,

(See figure on next page.)
Fig. 1 This figure displays the results of an in silico study. **A**-**E** The 2D illustrations of 5TR-1, MA3, S1.6, S2.2, and STRG2, respectively, providing a visual representation of their structures. **F**-**J** The 3D structures of these aptamers, offering a more detailed view of their spatial arrangement. **K**–**O** The molecular docking simulations between MUC1 and the aptamers, highlighting the predicted binding modes and interactions. Overall, this figure provides a comprehensive overview of the structural features and binding interactions of the investigated aptamers with MUC1. 2D, Two-dimensional; 3D, Three-dimensional; MUC1, Mucin 1
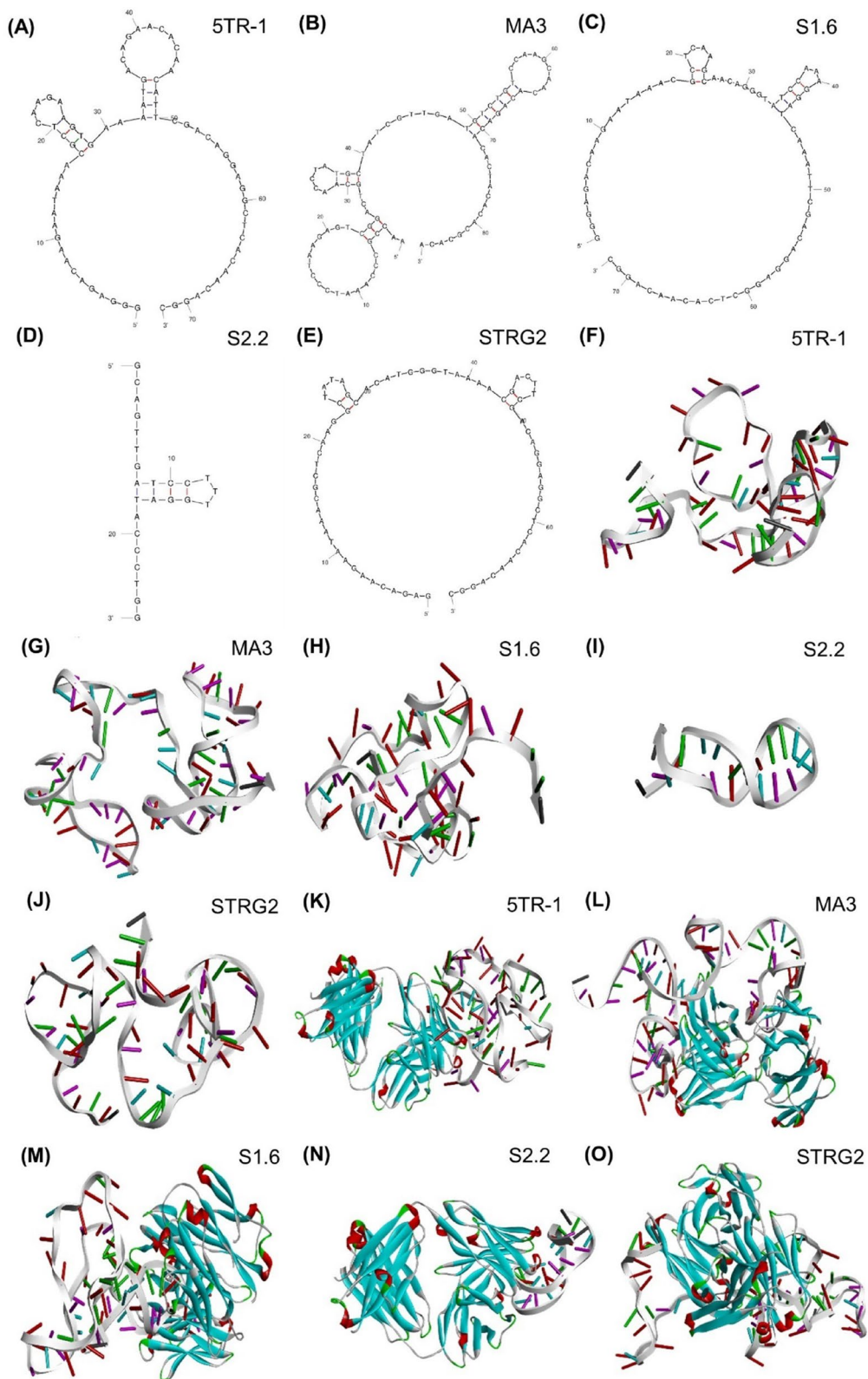
Fig. 1 (See legend on previous page.)

Khan *et al. Health Nanotechnology*   (2025) 1:2

Page 6 of 14

and confidence scores, S1.6 outperforms STRG2. Considering all the parameters assessed, it can be concluded that S1.6 is the most suitable aptamer among the options considered.

Liposome preparation

Figure 2A illustrates the schematic method for preparing an aptamer-conjugated liposome encapsulated with DOX. To synthesize the liposomes, we focused on three key factors: size, Poly dispersity index (PDI), and DOX encapsulation. We varied the molar ratios of DPPC (1,2-dipalmitoyl-sn-glycero-3-phosphocholine), cholesterol and DSPE-PEG-Mal (N-[(3-Maleimide-1-oxopropyl)aminopropyl polyethyleneglycol-carbamyl] distearoylphosphatidyl-ethanolamine) to determine the optimal combination. In our approach, we added 0.5 mg of DOX to the solvent and measured its absorption, which yielded a value of 0.595.

Table 2 presents the absorption values of several DL along with their encapsulation rates. After purification using a syringe filter and a size exclusion chromatography, we identified the formulation with the highest absorption value of 0.455, corresponding to a DOX amount of 0.412 mg within the liposomes as shown in Fig. 2B. We measured the DOX concentration using a UV–Vis spectrophotometer at a wavelength of 480 nm. Importantly, we achieved a high encapsulation rate of 73.39% with this liposome formulation, making it suitable for further experiments.

The size analysis revealed that our DL had an average size of approximately 84.86 nm, meeting our target size of less than 100 nm. We also confirmed the appropriate synthesis of the liposomes through Transmission electron microscopy (TEM) imaging as shown in Fig. 2C.

In summary, based on the absorption, encapsulation rate, and size analysis, we synthesized liposomes that effectively encapsulate DOX for our further experiments.

Aptamer conjugation

The efficiency of aptamer conjugation was determined using UV–Vis spectrophotometer, and the results are depicted in Fig. 2D. Before purification, the concentration of nucleic acid was measured as 152.5 ng/μl, while after purification, it reduced to 121.3 ng/μl, indicating a conjugation rate of 79.54%. To confirm aptamer conjugation, DLS measurements were performed to assess changes in size and charge. The graphical representation clearly illustrates the distinction between aptamer conjugated and non-conjugated samples. Figure 2E shows the alignment of aptamer conjugated liposomes, while Fig. 2F displays random and scattered patterns for non-conjugated liposomes.

Gel electrophoresis was conducted to further validate the conjugation process. Figure 2G presents the results for our five samples, where Liposome aptamer non-conjugated (LA–N) and Liposome-DOX aptamer non-conjugated (LDA-N) showed bands similar to the aptamer alone (S1.6). In contrast, there were no bands observed for the Liposome-aptamer (LA) and Liposome-DOX-aptamer (LDA), indicating the absence of free aptamer molecules.

Zeta potential measurements were performed to assess the surface charge of the liposomes. The values obtained were -0.26, -7.18, and -5.39 for liposomes, LA, and LDA, respectively. The negatively charged aptamer and positively charged DOX contribute to the observed differences in zeta potential.

Regarding stability, the LDA complex exhibited consistent size measurements at both 4℃ and 25℃, indicating its stability over time is detailed in Figure S4.

Cell line selection

The expression level of MUC1 was confirmed of using an anti-human MUC1 antibody through flow cytometry. While MCF7 cells are known to be MUC1-positive, previous literature suggested that MDA-MB-231 cells also exhibit MUC1 positivity. Surprisingly, our investigation revealed that MDA-MB-231 cells express MUC1

(See figure on next page.)

Fig. 2 A Schematic illustration of liposome preparation and aptamer conjugation, created with Biorender.com. **B** DOX encapsulation was confirmed by DOX absorbance (λ_{max} = 485 nm). It provides information on the presence of DOX before and after purification, indicating the encapsulation of DOX within the liposomes. **C** The proper synthesis of liposomes was observed through TEM imaging. The scale used is 200 nm, and the imaging was conducted using a high voltage of 120 kV. **D** UV–Vis spectrophotometer results illustrate the concentration of aptamers before and after purification by DNA absorbance (λ_{max} = 260 nm), confirming the conjugation and enabling the calculation of the conjugation rate. **E** DLS results present the volume PSD of conjugated and non-conjugated liposomes with aptamers, respectively. **F** DLS results present the volume PSD of conjugated and non-conjugated liposomes with aptamers, respectively. Conjugated aptamer-liposomes exhibit aligned peaks, while non-conjugated liposomes with aptamers display random and scattered peaks. **G** Gel electrophoresis results are presented, indicating the binding of aptamers with liposomes. LA and LDA show no bands, unlike LA–N and LDA-N, suggesting the successful conjugation of aptamers with liposomes. DOX, Doxorubicin; TEM, Transmission electron microscope; DLS, Dynamic light scattering; PSD, Particle size distribution; LA, Liposome-aptamer; LDA, Liposome-DOX-aptamer; LA–N, Liposome-aptamer non-conjugated; LDA-N, Liposome-DOX-aptamer non conjugated
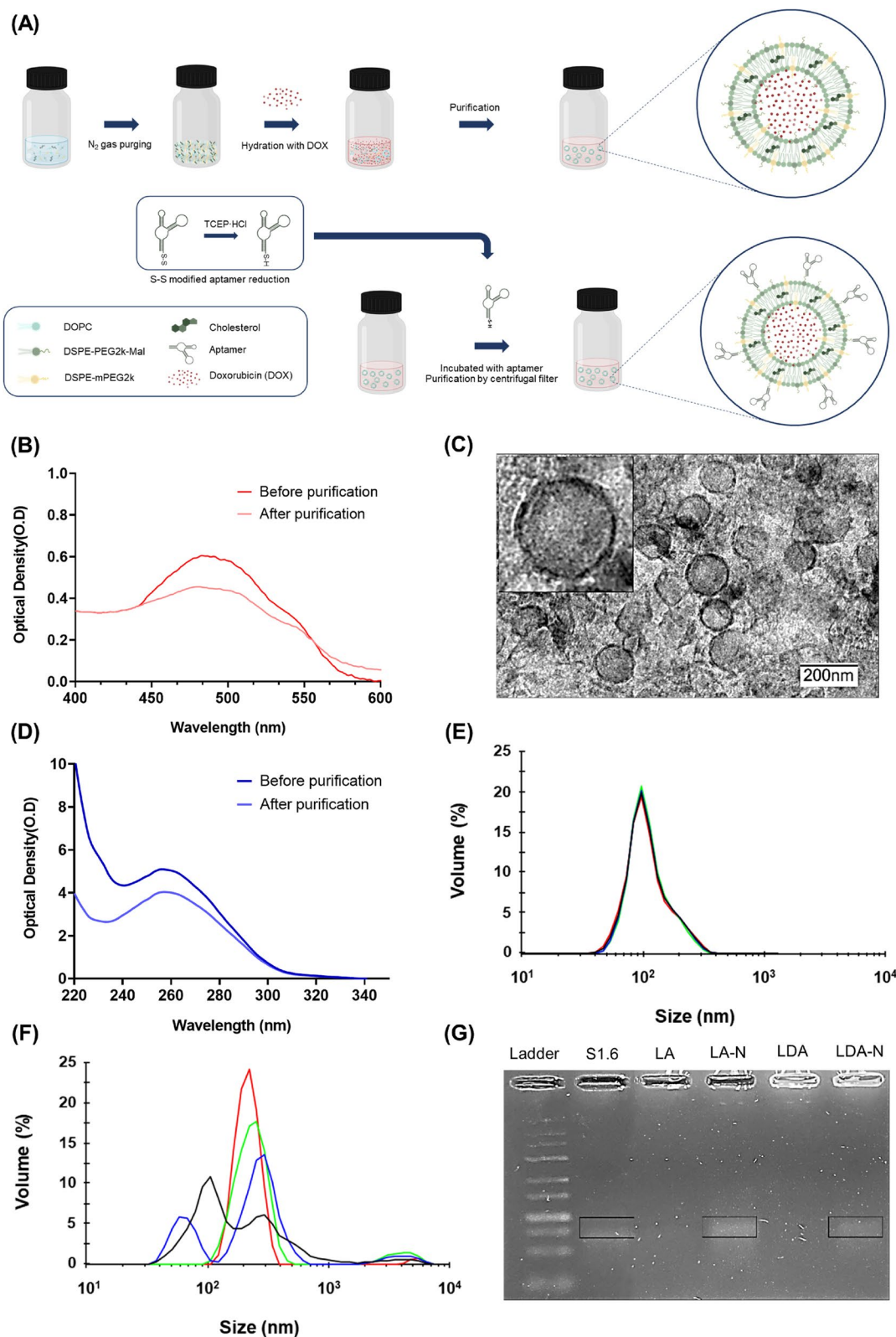
(A)

(B)

(C)

(D)

(E)

(F)

(G)

Fig. 2 (See legend on previous page.)

Table 2 Characteristics of liposomes based on lipid molar ratio

Molar Ratio	PBS (ml)	Abs (Before)	Abs (After)	Encapsulation rate	Size (nm)	PDI
15:9:1.0	2	0.612	0.060	9.80%	47.79	0.164
15:9:1.5	2	0.595	0.086	14.45%	50.73	0.147
12:8:1.0	2	0.623	0.046	7.38%	51.60	0.161
12:8:1.5	2	0.602	0.111	18.44%	51.98	0.163
10:6:1.0	2	0.586	0.208	35.49%	75.05	0.106
10:6:1.5	2	0.620	0.455	73.39%	84.86	0.166

The table provides information on the molar ratios utilized for liposome synthesis. It also includes the absorption scores before and after purification of DOX encapsulation by liposome. Additionally, the table presents the encapsulation rate of DOX, the size of the liposomes, and their PDI scores. *DOX* Doxorubicin, *PDI* Poly Dispersity Index
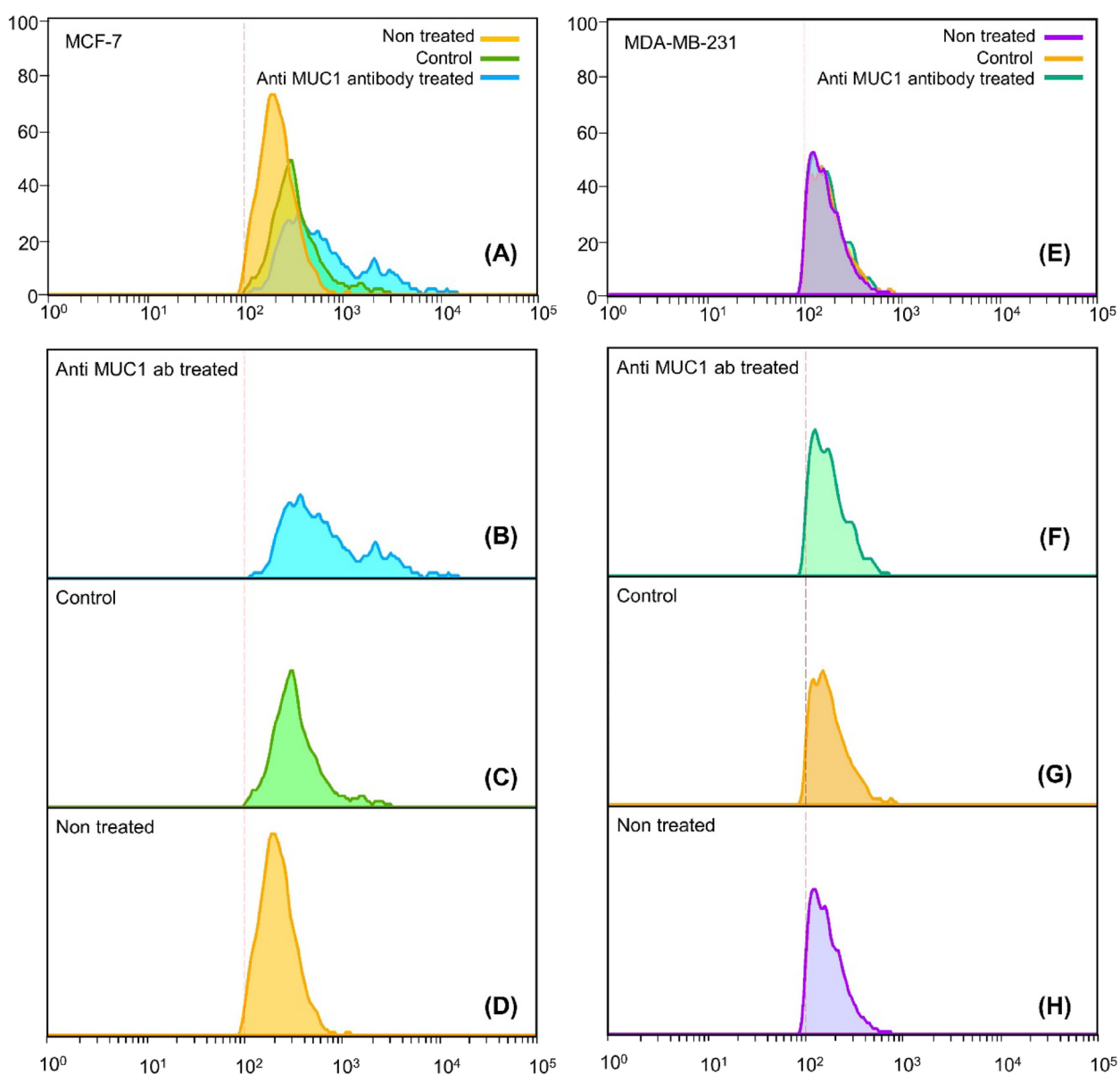

Fig. 3 Flow cytometry results of (**A**–**D**) MCF-7 cells and (**E**–**H**) MDA-MB-231 cells. **B**,**F** The results of anti-MUC1 antibody treatment on MCF7 and MDA-MB-231 cells. **C**, **G** The control and (D,H) non-treated cells. (A,E) The merged results of the treated, non-treated, and control cells

Khan *et al. Health Nanotechnology*   (2025) 1:2

Page 9 of 14

with a tandem repeat at extremely low levels as shown in Fig. 3F. The MUC1-targeting antibody used in our study, generated using a synthetic peptide representing a region near the beginning of the human MUC1 protein, potentially corresponding to the tandem repeat region, indicated negative MUC1 expression in MDA-MB-231 cells as determined by flow cytometry analysis. Consequently, we selected MDA-MB-231 cells as the negative cell line for our experiment, as our aptamer S1.6 specifically targets the tandem repeat region of the MUC1 extracellular domain.

In our study, we employed a primary antibody, rabbit anti-human MUC1, which can bind to human MUC1. The secondary antibody used was a fluorescence dye-conjugated antibody, specifically Goat anti-rabbit, enabling binding to the rabbit-derived primary antibody. This indirect staining method allowed us to investigate the specificity of the primary antibody for MUC1 to get better results at the binding of the anti-MUC1 antibody. The histogram data from Fig. 3 showcase three categories: "Non-treated" represents cells without any antibody treatment (Fig. 3D,H), "Control" denotes cells treated solely with the secondary antibody (Fig. 3C,G), and "Anti- MUC1 ab treated" signifies cells treated with both the primary and secondary antibodies (Fig. 3B,F). By examining the fluorescence intensity depicted on the X-axis of the graph, a shift towards the right indicates the binding of our fluorescence dye-conjugated antibody to the target antigen on the cells. Notably, the graph shifts in the "Anti- MUC1 ab treated" category is more pronounced compared to the "Control" and "Non-treated" groups, highlighting the specific binding of the primary antibody to MUC1 and the absence of nonspecific binding from the secondary antibody.

Cellular uptake study

The efficiency of aptamer-mediated DOX delivery by LDA was tested using confocal microscopy imaging in MCF-7 and MDA-MB-231 cells. In the case of cells alone, no DOX signal was detected. However, with DL or LDA treatment, DOX signals were observed in both cell lines. In DL treated cells, the DOX signal was similar between the two cell lines, whereas LDA treatment resulted in a significantly higher DOX signal in MCF-7 cells compared to MDA-MB-231 cells. Furthermore, the DOX signal was significantly higher in LDA treated cells compared to DL treated cells in MUC1-positive MCF-7 cells, confirming the enhanced DOX delivery by LDA. The absorption of liposomes increased over time, as indicated by the divergence in absorption rates between the 1-hour and 3-hour time points in the positive cell line for LDA. This emphasizes the enhanced

delivery of LDA mediated by the S1.6 aptamer compared to liposomes alone (Fig. 4).

Based on these results, it can be concluded that the S1.6 aptamer is an effective ligand for specifically targeting MUC1, as demonstrated by the distinct binding patterns observed between the positive and negative cell lines.

Conclusion

In conclusion, our study presents a promising strategy for improving the specificity and effectiveness of drug delivery while minimizing the harmful side effects on healthy tissues. By targeting the overexpressed MUC1 protein, we developed a DOX loaded platform conjugated with a carefully selected aptamer. A key aspect of our approach was the use of a comprehensive in-silico screening method to evaluate multiple MUC1-targeting aptamers. By assessing thermodynamic stability, docking score, confidence score, and binding affinity, we identified the most suitable aptamer for precise drug delivery.

Through in vitro experiments using MCF7 and MDA-MB-453 cells, we demonstrated the ability of our approach to selectively target MUC1-expressing cancer cells, providing evidence for the potential clinical utility of this technique. By enhancing the specificity of drug delivery to cancer cells, our approach holds promise in mitigating the non-specific toxicity associated with traditional chemotherapy.

While our results are encouraging, further studies are warranted to evaluate the therapeutic efficacy of this approach in vivo. Animal models can provide valuable insights into the biodistribution, pharmacokinetics, and overall therapeutic response of the aptamer-mediated liposomal encapsulation of chemotherapeutic agents. Additionally, comprehensive investigations should be conducted to assess the long-term effects and potential side effects of this novel approach.

Overall, with continued research and refinement, it is possible to overcome the limitations of conventional chemotherapy and significantly improve patient outcomes and quality of life. The development of innovative strategies like aptamer-mediated liposomal encapsulation, supported by the in silico screening of aptamers for optimal binding and stability, represents a crucial step toward personalized and more effective cancer treatment.

Experiential section

Materials

DPPC was obtained from Avanti Polar Lipids, located in Alabama, USA. Cholesterol, tris(2-carboxyethyl) phosphine hydrochloride (TCEP•HCl), DOX, Tris–Borate-EDTA (TBE), Bovine serum albumin(BSA) and chloroform were purchased from Sigma-Aldrich, based
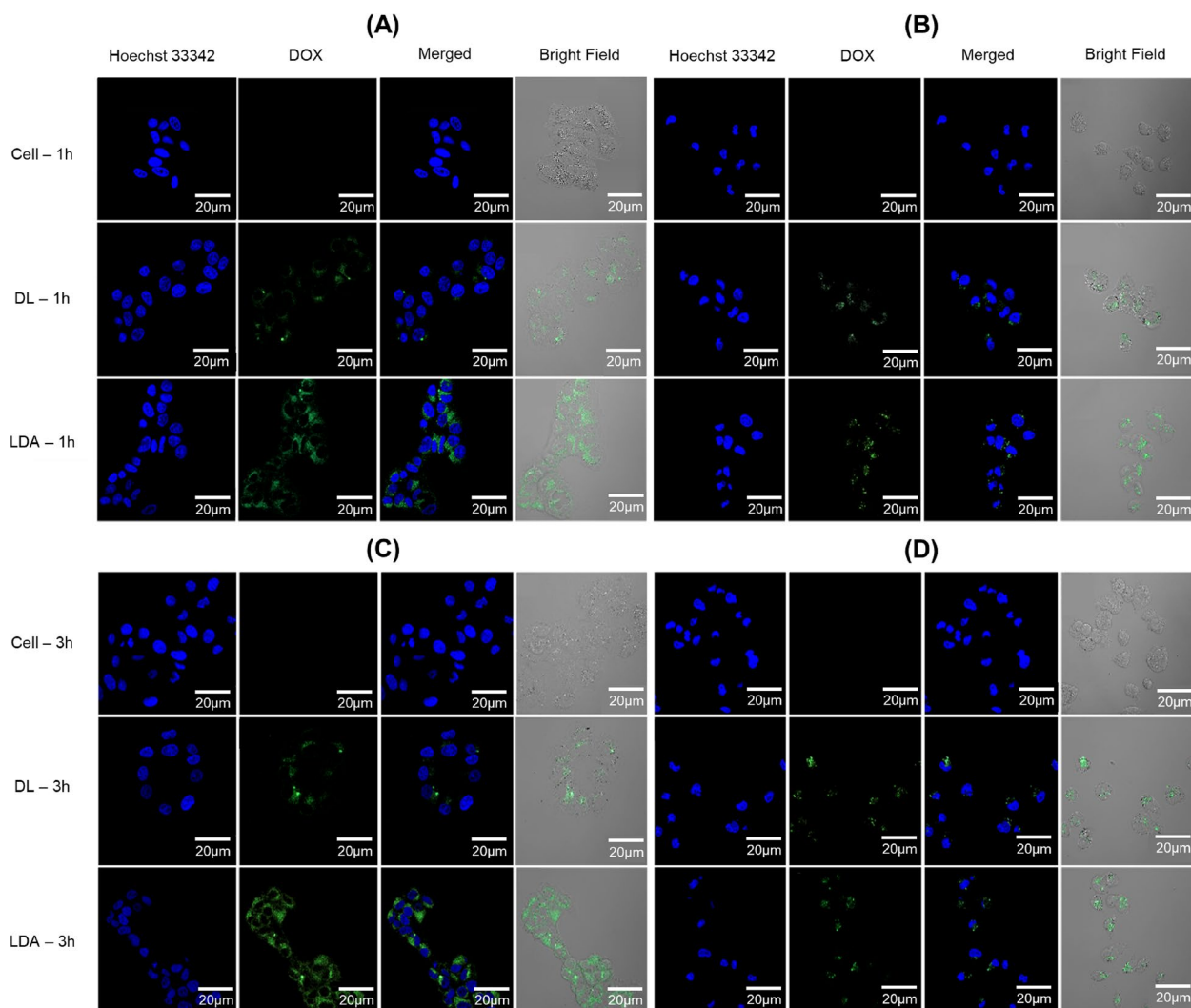
Khan *et al. Health Nanotechnology*   (2025) 1:2

Page 10 of 14

Fig. 4 This figure illustrates the findings of confocal imaging, where Hoechst 33,342 staining was employed to visualize the nucleus (represented by blue color) and DOX fluorescence (indicated by green color). **A** The imaging results of MCF7 cells after 1 hour. **B** The imaging results of MDA-MB-231 cells after 1 hour. **C** The imaging outcomes of MCF7 cells after 3 hours. **D** The imaging results of MDA-MB-231 cells after 3 hours. DOX, Doxorubicin; DL DOX-encapsulated liposome; LDA, Liposome-DOX-aptamer

in Seoul, Korea. DSPE-PEG-Mal was obtained from Creative PEGWorks, situated in North Carolina, USA. S1.6 with terminal disulfide modification (S1.6-SS) was purchased from Humanizing Genomics Macrogen, located in Seoul, Korea. MCF7 and MDA-MB-231 cell lines, along with the necessary supplies for the in vitro assay, were obtained from Korean Cell Line Bank located in Jong-no Gu, Seoul. The MUC1 (MUC1 (D9O8K) XP® Rabbit mAb #14161) antibody was purchased from Cell Signaling Technology, based in Massachusetts, USA. NanoDrop™ 2000/2000c spectrophotometer (Thermo Scientific™; ND-2000), Zetasizer Nano ZS (Malvern), flow cytometry (Guava® easyCyte™ 5, Luminex), and

Confocal Microscope Nikon ECLIPSE Ti2 (Tokyo, Japan) were used in our experiment.

Methodology

3D structural modeling of aptamers

To identify aptamers targeting the MUC1 protein and their binding affinity, we utilized the "Aptabase (www.iitg.ac.in/proj/aptabase)" as a resource Table 1. Binding affinity serves to evaluate and rank the strength of interactions between two molecules, which is expressed by the equilibrium dissociation constant (KD). A smaller KD value indicates a higher binding affinity, signifying a stronger attraction and interaction between the ligand and its target. Initially, we employed the

Khan *et al. Health Nanotechnology*   (2025) 1:2

Page 11 of 14

UNAFold Web Server (http://www.unafold.org/mfold/applications/dna-folding-form.php) to predict the 2D structure of the aptamers [41]. This web server utilizes thermodynamic calculations based on nearest-neighbor energy parameters to forecast the 2D structure of DNA. By analyzing the input DNA sequence, it determines stable secondary structures through considerations of base pairing interactions and the minimization of free energy within the system. For the analysis, we set the DNA sequence as linear, while the folding temperature was fixed at 37 °C to simulate physiological conditions. Additionally, the ionic conditions, including Na^+ and Mg^{2+} concentrations, were applied as detailed in Table 1. Furthermore, the correction type was selected as oligomer to account for the short length of the aptamer. All other parameters were left at their default values.

Subsequently, we utilized the Xiao Lab web server to design the 3D models of our aptamers [42, 43]. This web server applies common approaches in DNA structure prediction, including molecular dynamics simulations and constraint-based modeling. These techniques leverage experimental data to guide the prediction process. Specifically, we selected DNA as the molecular type and chose "optimized" as the procedure option. For minimizing and refining the 3D structure of the aptamers, we employed the Maestro 12.5 software, developed by Schrödinger. Following this step, the models were prepared and ready for further analysis and investigation.

Screening the aptamers by molecular docking

For the molecular docking between the aptamers and MUC1 protein, we employed the HDOCK server, which is well-known for its capability in DNA−protein molecular docking [44]. To initiate the process, we retrieved the 3D structure of the MUC1 protein from the RCSB Protein Data Bank (PDB) website. The specific PDB ID we used, was 7V64, which represented the protein in complex with an antibody. To prepare the MUC1 protein for molecular docking, we utilized the Maestro 12.5 software, developed by Schrödinger. With the software, we isolated the protein from the complex and added hydrogen molecules to optimize its structure.

The HDOCK server is known for generating multiple docking poses based on shape complementarity and electrostatic interactions. The algorithm of the server produced numerous docking processes, which were then evaluated using a scoring function to determine their compatibility and quality. The scoring function considered various factors such as shape complementarity, protein-DNA interface interactions, and energy terms [44].

On the server webpage, we uploaded the 3D structure of the MUC1 protein as the receptor molecule and the aptamers as the ligand molecule for the docking. The docking performed was template-free, meaning it did not rely on a predefined template. The HDOCK server provided us with 100 predicted docking results, out of which we analyzed the top 10 models. Through comparison with other aptamers, we confirmed that our S1.6 aptamer emerged as a promising candidate for use as a target-specific ligand.

Liposome preparation

The liposomes utilized in this study were prepared using the film hydration method. To create plain liposomes, a mixture consisting of DPPC, cholesterol, and DSPE-PEG-Mal in a molar ratio of 10:6:1.5 was dissolved in a mixture of chloroform and methanol in a 2:1 volume-to-volume ratio [2, 45]. We employed several molar ratios to determine the optimal encapsulation of DOX, as indicated in Table 2.

Subsequently, the solvent was evaporated using a stream of nitrogen gas, and the resulting lipid film was placed in a high vacuum overnight to remove any remaining organic solvent. To hydrate the lipid film, we used a PBS solution along with DOX. Tip sonication was employed at room temperature to facilitate the hydration process [46]. Any non-encapsulated DOX and unwanted residues were eliminated by passing the liposome suspension through a syringe filter with a pore size of 0.20 μm. Additionally, a size exclusion chromatography with a bed volume of approximately 2.5 mL was utilized for further purification [6].

To determine the encapsulation rate of DOX, we employed a UV–Vis spectrophotometer which is a specialized instrument capable of measuring the absorbance and concentration of various biomolecules, including nucleic acids and proteins. It emits a broad-spectrum light beam that passes through the sample, and the transmitted light intensity is measured.

Following purification, the final concentration of DOX was determined using the UV–Vis spectrophotometer. By dividing the final concentration by the initial concentration and multiplying by 100, we obtained the percentage of encapsulation for DOX.

Conjugation of S1.6 to liposomes

Aptamers are highly specific and exhibit a strong affinity for their molecular targets, making them valuable in active targeting and personalized medicine to minimize off-target effects. Additionally, disulfide bonds present in aptamers are prone to oxidative dimerization, forming disulfide bonds that impede their reaction with

Khan *et al. Health Nanotechnology*   (2025) 1:2

Page 12 of 14

maleimides. To overcome this challenge, pre-reduction of disulfide bonds and exclusion of oxygen is necessary. In our study, we utilized TCEP•HCl reagent for disulfide reduction [47, 48].

Initially, we performed the folding process of the aptamer to enable it to adopt a specific 3D structure. It was mixed with a buffer solution containing 0.2 M NaHCO3 and 0.5 M NaCl at a two-fold concentration, in a 1:1 molar ratio. The mixture was heated to 95 ℃ for 10 min to denature the aptamer and then cooled down for 15 min at room temperature [48, 49].

For conjugating the S1.6-SS to the surface of liposomes, a method adapted from Li et al. was employed [50]. The liposomes, which had DSPE-PEG-Mal on their surface, were incubated with S1.6-SS at a ratio of 5:1 for 1 h. The reaction took place in the presence of TCEP•HCl at a pH range of 6–8, and the reaction was conducted in the dark at room temperature with moderate stirring. TCEP•HCl served as a reducing agent to facilitate the reductive reaction between the disulfide bonds of the aptamers and the maleimide groups on the surface of the liposomes [48, 50].

Characterization

The efficiency of conjugation between S1.6 aptamer and liposomes was determined by measuring the aptamer concentration before and after washing using the UV–Vis spectrophotometer. To wash the conjugated samples, a 30 kDa centrifuge filter tube was used, and the washing process was performed at 4000 rpm for four cycles. Additionally, DLS data was utilized to confirm the conjugation. DLS involves directing a laser beam at the sample and analyzing the scattered light to extract information about the Brownian motion of the particles, which is related to their size. By analyzing the Intensity Particle size distribution (PSD), Volume PSD, and Number PSD of the S1.6 aptamer only, liposome only, LA–N, and LA, the proper conjugation was confirmed.

Furthermore, electrophoretic mobility measurements were conducted using DLS to determine the velocity at which the particles move under an electric field. This information provided insights into the charge of the particles. The difference in zeta potential before and after conjugation also served as an indicator of conjugation.

To evaluate the stability of the aptamer-liposome complex, data was collected at various time intervals (0, 1, 3, 5, and 7 days) under storage conditions of 4 ℃ and 25 ℃. This assessment aimed to understand the changes in the particle size, PDI, and zeta potential over time, which are indicative of the stability and potential aggregation of the complex.

For examining the microstructure and morphology of the liposomal vesicles, TEM was employed. TEM samples were prepared by placing a drop of diluted liposome dispersion onto a TEM grid and allowing it to air dry [51]. The images were captured using an accelerating voltage of 120 kV. This energy level was chosen to achieve sufficient electron penetration while minimizing sample damage, ensuring optimal visualization of the liposomes' characteristics.

Gel electrophoresis was conducted using a 3% TBE gel to confirm the liposome and aptamer conjugation [52]. The electrophoresis process was carried out for 80 min at 50 V in 1X TBE buffer. The gel's pore size was suitable for separating DNA fragments of different sizes, allowing the visualization and confirmation of the conjugated aptamer with the liposomes. TBE buffer was used to maintain the stability and integrity of the DNA throughout the electrophoresis process.

Analyzing MUC1 expression

The assessment of MUC1 expression in cancer cell lines is crucial for targeting the cell line. We employed immunofluorescence staining to investigate the presence of MUC1 in MCF7 (MUC1 positive) and MDA-MB-231 (MUC1 negative) cell lines. The experimental procedure involved cell seeding, antibody treatment, washing steps, and fluorescence imaging. We utilized the rabbit anti-human MUC1 antibody as the primary antibody and a fluorescence dye-conjugated goat anti-rabbit antibody as the secondary antibody [22]. To ensure optimal conditions for staining, a 5% BSA PBS buffer was prepared for cell washing and resuspension. The cells were first washed with DPBS and detached using Trypsin–EDTA, followed by cell counting and centrifugation. Subsequently, the cells were resuspended in 100 μL of 5% BSA PBS buffer. For MUC1 detection, the cells were treated with the primary antibody (0.25 μg/tube) and incubated in dark conditions at 4 ℃ for 30 min. After three washes with ice-cold 5% BSA PBS solution, the cells were subjected to the secondary antibody treatment and incubated under the same conditions. Finally, the cells were washed again, and flow cytometry analysis was used to visualize the MUC1 expression pattern. This study provides valuable insights into the MUC1 status in MCF7 and MDA-MB-231 cell lines.

Receptor-mediated cellular uptake

The binding specificity of LDA in the MCF7 MUC1 positive cell line and the MDA-MB-231 negative cell line was evaluated using a confocal microscope. Three samples were analyzed: Cells only, DL, and LDA, to identify any differences. Images were captured at 1-hour and 3-hour intervals.

MCF7 cells were cultured in the DMEM medium, while MDA-MB-231 cells were cultured in the RPMI medium. Both media were supplemented with 10% fetal bovine serum and 1% antibody. The cells were maintained in a humidified incubation chamber at 37°C and pH 7.4 with 5% CO_2.

For the analysis of receptor-mediated cellular uptake of the liposomes, confocal imaging was employed using DOX as a fluorescent compound. MCF7 and MDA-MB-231 cells were seeded onto confocal dishes at a density of 1×10^5 cells and incubated at 37°C. After 24 h, the cells were washed with PBS, and 2 mL of media was added. Subsequently, the cells were treated with DL and LDA (100 µL each) and further incubated at 37°C. Live cell images and fixed cell images were captured at 1-h and 3-h time intervals. To visualize the cell nuclei, Hoechst 33342 dye was used for nuclear staining. For fixed cells, the cells were washed with PBS and fixed with 4% paraformaldehyde (w/v) diluted in PBS at room temperature. In the case of live cells, after washing, each confocal dish was filled with 2 mL of media. Confocal laser scanning microscopy was utilized to observe the nuclear location and cellular uptake of DOX [45].

Abbreviations

DOX	Doxorubicin
MUC1	Mucin 1
DLS	Dynamic light scattering
PEG	Poly ethylene glycol
EPR	Enhanced permeability and retention
2D	Two-dimensional
3D	Three-dimensional
PDI	Poly dispersity index
DPPC	1,2-Dipalmitoyl-sn-glycerol-3-phosphocholine
DSPE-PEG-Mal	N-[(3-Maleimide-1-oxopropyl)aminopropyl polyethylenegly-col-carbamyl] distearoylphosphatidyl-ethanolamine
DL	DOX-encapsulated liposome
LA–N	Liposome aptamer non-conjugated
LDA-N	Liposome-DOX aptamer non-conjugated
LA	Liposome-aptamer
LDA	Liposome-DOX-aptamer
TEM	Transmission electron microscope
PDB	Protein data bank
TCEP•HCL	Tris(2-carboxyethyl)phosphine hydrochloride
S1.6-SS	S1.6 with terminal disulfide modification
TBE	Tris–Borate-EDTA
BSA	Bovine serum albumin
PBS	Phosphate-buffered saline
KD	Equilibrium dissociation constant
PSD	Particle size distribution

Supplementary Information

The online version contains supplementary material available at https://doi.org/10.1186/s44301-024-00001-1.

Supplementary Material 1.

Authors' contributions
MSAK, JP, and SL contributed equally to this work, proposing the conceptual idea, conducting all studies mentioned in the article, and collectively contributing to the writing of the paper. H.I. designed and directed the research, analyzed the data, and revised the paper. HJ, CO, MK, JS, SGL, JJ, BP, and HNJ participated in laboratory meetings and advised study designs.

Data availability
No datasets were generated or analysed during the current study.

Declarations

Competing interests
The authors declare no competing interests.

Author details
[1]Department of Molecular Medicine and Biopharmaceutical Sciences, Graduate School of Convergence Science and Technology, Seoul National University, Seoul 08826, Republic of Korea. [2]Department of Applied Bioengineering, Graduate School of Convergence Science and Technology, Seoul National University, Seoul 08826, Republic of Korea. [3]Cancer Research Institute, Seoul National University, Seoul 03080, Republic of Korea. [4]Research Institute for Convergence Science, Seoul National University, Seoul 08826, Republic of Korea.

References

1. Jain RK, Stylianopoulos T. Delivering nanomedicine to solid tumors. Nat Rev Clin Oncol. 2010;7(11):653–64.
2. Cadinoiu AN, et al. Aptamer-functionalized liposomes as a potential treatment for basal cell carcinoma. Polymers. 2019;11(9):1515.
3. Kaasgaard T, Andresen TL. Liposomal cancer therapy: exploiting tumor characteristics. Expert Opin Drug Deliv. 2010;7(2):225–43.
4. Huwyler J, Drewe J, Krahenbuhl S. Tumor targeting using liposomal antineoplastic drugs. Int J Nanomedicine. 2008;3(1):21–9.
5. Torchilin V. Tumor delivery of macromolecular drugs based on the EPR effect. Adv Drug Deliv Rev. 2011;63(3):131–5.
6. Oh C, et al. Development of spleen targeting H(2)S donor loaded liposome for the effective systemic immunomodulation and treatment of inflammatory bowel disease. ACS Nano. 2023;17(5):4327–45.
7. Moosavian SA, Sahebkar A. Aptamer-functionalized liposomes for targeted cancer therapy. Cancer Lett. 2019;448:144–54.
8. Kim M, et al. Aptamer-conjugated nano-liposome for immunogenic chemotherapy with reversal of immunosuppression. J Control Release. 2022;348:893–910.
9. Maliyappa MR, et al. Synthesis, characterization, pharmacological and computational studies of 4, 5, 6, 7-tetrahydro-1, 3-benzothiazole incorporated azo dyes. J Mol Struct. 2019;1179:630–41.
10. Olusanya TOB, et al. Liposomal drug delivery systems and anticancer drugs. Molecules. 2018;23(4):907.
11. Petersen GH, et al. Meta-analysis of clinical and preclinical studies comparing the anticancer efficacy of liposomal versus conventional non-liposomal doxorubicin. J Control Release. 2016;232:255–64.

Khan *et al. Health Nanotechnology*   (2025) 1:2

Page 14 of 14

12. Mo T, et al. Aptamer-based biosensors and application in tumor theranostics. Cancer Sci. 2022;113(1):7–16.
13. Levy-Nissenbaum E, et al. Nanotechnology and aptamers: applications in drug delivery. Trends Biotechnol. 2008;26(8):442–9.
14. Zhou G, et al. Aptamers: a promising chemical antibody for cancer therapy. Oncotarget. 2016;7(12):13446–63.
15. Xiang D, et al. Superior performance of aptamer in tumor penetration over antibody: implication of aptamer-based theranostics in solid tumors. Theranostics. 2015;5(10):1083–97.
16. Lao YH, Phua KK, Leong KW. Aptamer nanomedicine for cancer therapeutics: barriers and potential for translation. ACS Nano. 2015;9(3):2235–54.
17. Chapman AP. PEGylated antibodies and antibody fragments for improved therapy: a review. Adv Drug Deliv Rev. 2002;54(4):531–45.
18. Jayasena SD. Aptamers: an emerging class of molecules that rival antibodies in diagnostics. Clin Chem. 1999;45(9):1628–50.
19. Gao T, Cen Q, Lei H. A review on development of MUC1-based cancer vaccine. Biomedicine. 2020;132:110888.
20. Hanisch FG, Muller S. MUC1: the polymorphic appearance of a human mucin. Glycobiology. 2000;10(5):439–49.
21. Kufe DW. MUC1-C oncoprotein as a target in breast cancer: activation of signaling pathways and therapeutic approaches. Oncogene. 2013;32(9):1073–81.
22. Maleki F, Rezazadeh F, Varmira K. MUC1-targeted radiopharmaceuticals in cancer imaging and therapy. Mol Pharm. 2021;18(5):1842–61.
23. Zelasko-Leon DC, Fuentes CM, Messersmith PB. MUC1-targeted cancer cell photothermal ablation using bioinspired gold nanorods. PLoS ONE. 2015;10(7):e0128756.
24. Pillai K, et al. MUC1 as a potential target in anticancer therapies. Am J Clin Oncol. 2015;38(1):108–18.
25. Chen W, et al. MUC1: structure, function, and clinic application in epithelial cancers. Int J Mol Sci. 2021;22(12):6567.
26. Li Y, Cozzi PJ. MUC1 is a promising therapeutic target for prostate cancer therapy. Curr Cancer Drug Targets. 2007;7(3):259–71.
27. Chen ML, et al. Simultaneous imaging of cancer biomarkers in live cells based on DNA-engineered exosomes. Analyst. 2021;146(5):1626–32.
28. He J, et al. Recent progress of aptamer-drug conjugates in cancer therapy. Acta Pharm Sin B. 2023;13(4):1358–70.
29. He S, et al. Advances in aptamer-mediated targeted delivery system for cancer treatment. Int J Biol Macromol. 2023;238:124173.
30. Garcia Melian MF, et al. Aptamer-based immunotheranostic strategies. Cancer Biother Radiopharm. 2023;38(4):246–55.
31. Moosavian SA, et al. 5TR1 aptamer-PEGylated liposomal doxorubicin enhances cellular uptake and suppresses tumour growth by targeting MUC1 on the surface of cancer cells. Artif Cells Nanomed Biotechnol. 2018;46(8):2054–65.
32. Kim DM, et al. Anti-MUC1/CD44 dual-aptamer-conjugated liposomes for cotargeting breast cancer cells and cancer stem cells. ACS Appl Bio Mater. 2019;2(10):4622–33.
33. Lee D, et al. Self-assembled DNA-protein hybrid nanospheres: biocompatible nano-drug-carriers for targeted cancer therapy. ACS Appl Mater Interfaces. 2022;14(33):37493–503.
34. Guo F, et al. Enhancement of thermal damage to adenocarcinoma cells by iron nanoparticles modified with MUC1 aptamer. J Nanosci Nanotechnol. 2016;16(3):2246–53.
35. Mohapatra S, et al. Synergistic anticancer effect of peptide-docetaxel nanoassembly targeted to tubulin: toward development of dual warhead containing nanomedicine. Adv Healthc Mater. 2017;6(2):1600718.
36. Vivo-Llorca G, et al. MUC1 Aptamer-capped mesoporous silica nanoparticles for navitoclax resistance overcoming in triple-negative breast cancer. Chemistry. 2020;26(69):16318–27.
37. Nosrati R, et al. Targeted SPION siderophore conjugate loaded with doxorubicin as a theranostic agent for imaging and treatment of colon carcinoma. Sci Rep. 2021;11(1):13065.
38. Yazdian-Robati R, et al. Smart delivery of epirubicin to cancer cells using aptamer-modified ferritin nanoparticles. J Drug Target. 2022;30(5):567–76.
39. Santini BL, et al. In silico design of novel mutant anti-MUC1 aptamers for targeted cancer therapy. J Chem Inf Model. 2020;60(2):786–93.
40. Rhinehardt KL, Srinivas G, Mohan RV. Molecular dynamics simulation analysis of anti-MUC1 aptamer and mucin 1 peptide binding. J Phys Chem B. 2015;119(22):6571–83.
41. Zuker M. Mfold web server for nucleic acid folding and hybridization prediction. Nucleic Acids Res. 2003;31(13):3406–15.
42. Zhao Y, et al. Automated and fast building of three-dimensional RNA structures. Sci Rep. 2012;2:734.
43. Zhang Y, Y Xiong, Y Xiao, 3dDNA: A Computational Method of Building DNA 3D Structures. Molecules, 2022. 27(18).
44. Yan Y, et al. The HDOCK server for integrated protein-protein docking. Nat Protoc. 2020;15(5):1829–52.
45. Liao ZX, et al. An AS1411 aptamer-conjugated liposomal system containing a bubble-generating agent for tumor-specific chemotherapy that overcomes multidrug resistance. J Control Release. 2015;208:42–51.
46. Mody S, Joshi A. Age-related macular degeneration and its association with neurodegenerative disorders. Cureus. 2023;15(2):e34920.
47. Dieguez-Acuña FJ, Woods JS. Inhibition of NF-κB-DNA binding by mercuric ion: Utility of the non-thiol reductant, tris(2-carboxyethyl)phosphine hydrochloride (TCEP), on detection of impaired NF-κB-DNA binding by thiol-directed agents. Toxicol in Vitro. 2000;14(1):7–16.
48. Wu R, et al. Effects of Small Molecules on DNA Adsorption by Gold Nanoparticles and a Case Study of Tris(2-carboxyethyl)phosphine (TCEP). Langmuir. 2019;35(41):13461–8.
49. Ferreira CSM, Matthews CS, Missailidis S. DNA aptamers that bind to MUC1 tumour marker: design and characterization of MUC1-binding single-stranded DNA aptamers. Tumor Biol. 2006;27(6):289–301.
50. Li L, et al. Nucleolin-targeting liposomes guided by aptamer AS1411 for the delivery of siRNA for the treatment of malignant melanomas. Biomaterials. 2014;35(12):3840–50.
51. Berger N, et al. Filter extrusion of liposomes using different devices: comparison of liposome size, encapsulation efficiency, and process characteristics. Int J Pharm. 2001;223(1–2):55–68.
52. Orban L, Chrambach A. Discontinuous buffer system for polyacrylamide and agarose gel electrophoresis of DNA fragments. Electrophoresis. 1991;12(4):233–40.

Publisher's Note